ISSN: 0067-2904

The Effects of Psi Morphology on the Detection Efficiency of the Au-Nps Hot Spot SERS Sensors

Mohammed J. Mahmood[1], Alwan M. Alwan*[2]
[1]Directorate medical services, Agency of ministry for administration affairs, Ministry of interior, Baghdad, Iraq
[2]Department of Applied Sciences, University of Technology, Baghdad, Iraq

Received: 10/3/2020 Accepted: 28/5/2020

Abstract

This work is related to the investigation of the effects of porous silicon (PSi) morphologies on the performance of plasmonic gold nanoparticles (Au-NPs) hot spot SERS sensors for the detection of amoxicillin molecules. Two Si wafers with different resistivity values of 10 and 100 Ω.cm were used to synthesize a PSi layer of pores- and mud-like structures, respectively, by pulsed photo chemical etching process. The hot spot SERS sensors were synthesized by incorporating the Au-NPs within the PSi morphologies of pores- and mud- like structures which are characterized by high density of nucleation sites. Plasmonic Au- NPs with different sizes and hot spot regions were incorporated into the porous structures by the ion reduction process. It was recognized that the PSi morphologies have a considerable influence on the fabrication process of the detection sensors and, consequently, on the detection process. The plasmonic Au-NPs hot spot SERS sensor based on the PSi morphology of the mud-like structures shows higher sensitivity than that of pores-like structures, even at very low concentrations of amoxicillin solutions.

Keywords: SERS; Plasmonics Au-NPs; Hot spot gaps; Porous silicon morphology; Amoxicillin.

دراسة عن تأثير مورفولوجيا السليكون المسامي على كفاءة الكشف للحساسات (Au–NPs hot spot SERS)

محمد جمال محمود[1] ,علوان محمد علوان*[2]
[1]دائرة الخدمات الطبية, الشوؤن الادارية, وزارة الداخلية, بغداد, العراق
[2]قسم العلوم التطبيقية, الجامعة التكنولوجية, بغداد، العراق

الخلاصة

تم انجاز هذا العمل لغرض دراسة تأثير تشكيلية السليكون المسامي على اداء المتحسس ذات البقع الساخنة الواقعة بين جسيمات الذهب النانوية بطريقة تدعيم تشتت رامان للسطح واستخدام هذا المتحسس للكشف على الاموكسيسيلين. ان طبقتي السيليكون المسامي ذات التركيب بالشكل المسامي والرقع الطينية المتكون بطريقة التحفير الكيميائي بواسطة الليزر النبضي باستخدام شريحتي سيليكون ذات مقاومية (10 و100)اوم–سم على التوالي .هذا المتحسس ذات البقع الساخنة استخدمت فيه عملية دمج جسيمات الذهب النانوية ضمن تشكيلة التركيب ذات الشكل المسامي والتركيب ذات الرقع الطينية والتي تتميز بالكثافة العالية لمواقع نويات الذهب .

*Email: alkrzsm@yahoo.com.

تم الحصول على جسيمات الذهب النانوية ومناطق ا لبقع الساخنة باحجام مختلفة بدمجها داخل التركيب المسامي بعملية الاختزال الايوني حيث تم الاستشعار بان السليكون المسامي بتركيبيه ذات تاثير كبير على الكشف للمتحسس المصنع . ان الكاشف المكون من القاعدة ذات تركيب الرقع الطينية يحتوي على تحسسيه عالية مقارنة بالكاشف المكون من القاعدة ذات التركيب المسامي حتى مع التراكيز القليلة لمحلول السيليكون .

1-Introduction

The surface-enhanced Raman scattering (SERS) process was used to enhance the scattering effect and overcome the low sensitivity of the common Raman method. This process significant to distinguish the chemical and biochemical segments, by acting as a powerful process for the detection of various analytes[1,2]. Recently, SERS has been also efficiently used in evaluating food safety and quality, including fast detection of different types of antibiotics [3-7]. SERS is an enhancement of the Raman signal activity to several orders of magnitude. This enhancement is mainly due to the interaction between light and metallic nanoparticles, which is linked to the effects of Plasmon nanoparticles and hot spot regions [8]. Typically, in SERS sensors, the plasmonics nanoparticles such as gold (Au) or silver (Ag) were employed to enhance Raman signal intensity and lower the detection limits of the fabricated sensors [9-11].

The SERS sensor mainly consists of plasmonics nanoparticles incorporated on a based substrate. One of the most popular and significant substrates for developing this type of chemical sensors is the PSi [12,13]. The structural properties (surface morphology, silicon nanocrystallites, and the amount of nucleation sites) are the very specific parameters for the formation of the plasmonic nanoparticles for the sensor. The PSi morphology is the most particular formation factor for controlling the size of the plasmonic nanoparticle and the density of the hot spot regions, since the density of the dangling bonds (metallic nucleation sites) varies with the type of the morphologies [14,15]. The pores-like and mud-like structures of PSi have different topographical patterns and vary with the formation conditions of the PSi layer [16,17]. In this study, efficient SERS plasmonic Au-NPs hot spot sensors were fabricated and the effects of Psi morphologies on the performance of these sensors were studied at very low concentrations of amoxicillin molecules.

2- Experimental part

The formation of the PSi substrate was carried out through the etching process of n-type Si in a cell made of teflon at room temperature. The etching solution consists of ethanol (C_2H_5OH) and hydrofluoric acid (HF) in a ratio of 2 to 1. The PSi layer of pores- and mud- like structures were synthesized via the pulsed photochemical etching process by using two different silicon wafer resistivity values of 10 and 100 Ω.cm, respectively. For the n-type doped Si, light must be provided since holes are wasted during the etching process. The holes play a significant role in Si etching. The reaction of dissolution creates defects on the surface of the silicon wafer surface, pores will be formed, and their walls will be eroded until they are removed from the holes. Laser pulse duty cycle, 30% of laser wavelength of 405 nm, and laser intensity of 100mW/cm^2 were employed in the etching process at a fixed etching time of 40 min. The schematic representation of the pulsed photochemical etching process is illustrated in Figure-1. Plasmonic Au- NPs with different sizes and hot spot regions were incorporated into the porous structures by ion reduction (immersion) process. This process was accomplished at room temperature with a fixed concentration of $HAuCl_4$ of about $5x10^{-3}$M and an immersion time of 100 sec. The characterization of the based PSi substrate and SERS plasmonic Au-NPs hot spot sensors was carried out by measuring the FE-SEM images, photoluminescence's spectrum PL, and SERS spectra. The FE-SEM was investigated via a MIRA3 TESCAN field-emission scanning electron microscope, the PL spectrum was scanned by PL (Cary Eclipse FL 0912M014), and Raman measurements were examined using RENISHAW Raman scope 2000 device.

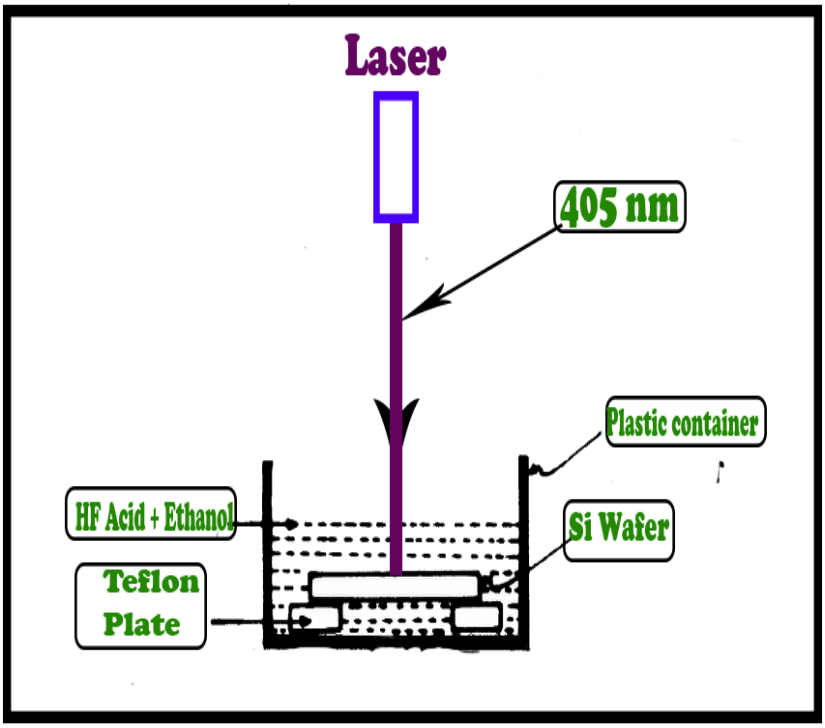

Figure 1-Schematic representation of the pulsed photochemical etching process.

3- Results and discussions

3-1 Morphological properties of the based PSi layer

Morphological aspects (pore shape, size, and nature) of the PSi layer were studied according to the values of the silicon wafer resistivity. Two specific types of morphologies of ultra-fine pores - like and mud- like structures were achieved for two different values of Si wafer resistivity (10 and 100 Ω.cm, respectively), as shown in Figure-2a, b. These structures have unique features in adjusting the parameters of the plasmonic Au-NPs layer deposited over the based PSi layer. The porosity and PSi layer thickness were determined based on the gravimetric method [18]. The porosity values of mud- and pores- like PSi structures were about 45% and 30%, respectively. The values of the PSi layer thickness were about 150 nm and 270 nm for pores- and mud- like structures, respectively.

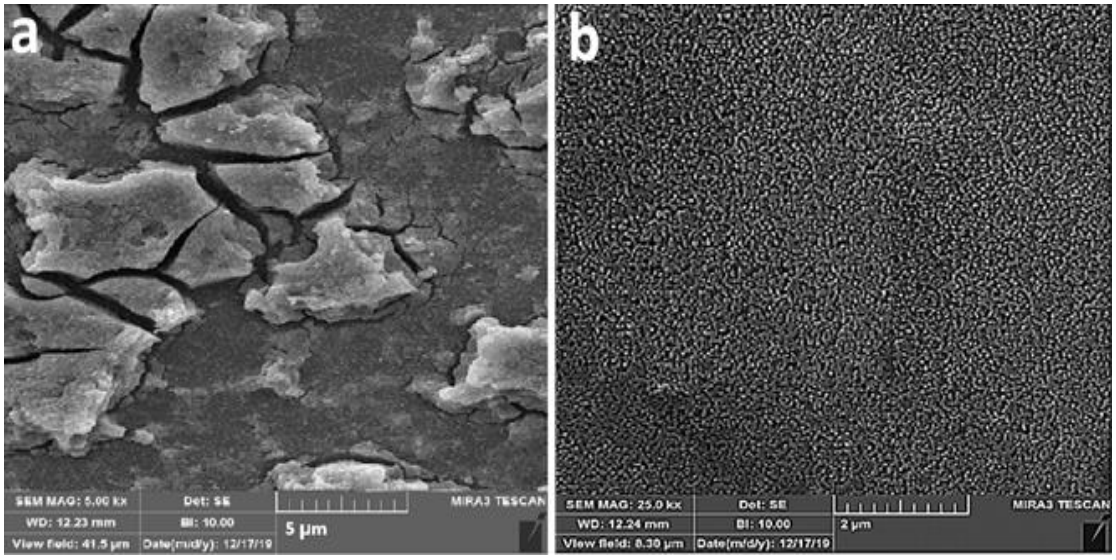

Figure 2-Surface morphology of the based PSi layer of Si wafer with resistivity values of a) 100 Ω.cm and b) 10 Ω.cm.

For silicon wafer with resistivity of 100 **Ω**.cm, Figure-2a shows that the surface of bulk Si was reconstructed into micro island regions named mud-like structures. This type of PSi morphology is

characterized by high density of Si hydrogenated bonds (Si- H_x) with x=2, 3. [19,20]. This structure is related to the doping of the Si wafer. As the doping decreases with increasing the wafer resistivity, the etching process was carried out strongly on the surface of silicon in x and y directions rather than deeply across the depth of wafer (in Z-direction). For Si wafer of resistivity of 10 Ω.cm, the surface of the Si was converted to pores -like structures (Figure-2b). One can observe that the surface morphology includes the existence of very tiny pores (pores -like structures). Among these pores, there are silicon nano column regions with different sizes. The formation of this type of morphology is due to the increase in the etching rate in the z-direction deeply into the silicon wafer. As the doping increases with the decrease of the wafer resistivity, the availability of silicon atoms in the laser irradiated area was dropped and, therefore, the etching rate was maintained in the lower silicon layer.

3-2 Optical properties of the based PSi layer

The optical properties of the based PSi layer were examined by analyzing the photoluminescence spectra. The Si nano crystallite size (L) and the energy gap of the PSi layer (E_{gPSi}) are related with the bulk Si energy gap (1.12 eV) by the following equation [18]:

$$\mathbf{E_{gPSi} = E_{gSi} + \frac{88.34}{L^{1.37}}} \quad \textbf{(1)}$$

The E_{gPSi} is realized directly from the peak of the PL emission corresponding to the maximum wavelength (**λmax**) and, thus, E_{gPSi}, (eV) = hc/λ_{max}. Figure-3 shows the PL spectra of both types of PSi morphologies (mud- and pores- like structures). From this figure, it is observed that the PL peaks are located at wavelengths of 638 and 680 nm, corresponding to the emission spectrum of PSi. The intensity and the full width at half maximum (FWHM) of the PL spectrum vary with the types of porous morphology. The PL spectra of the mud-like structure sample have lower FWHM compared with that of the PL spectra of the pores-like structure sample, while the PL peak intensity of the mud-like structure is higher than that of the pores- like structure sample. This broadening of the FWHM of PL spectra is increased with the dispersion of Si nano crystallites within the porous matrix. The PL peak intensity is increased with increasing the density of silicon nano crystallites. The values of L, λ_{max}, and EgPSi for mud- and pores- like structures are tabulated in Table-1. This variation in the obtained results from PL spectra is related intensively with the morphology of the based PSi layer. The formed mud-like PSi structure is a specific form of PSi morphology that includes high density of silicon nano crystallites (high density of gold nucleation sites) [18]. The high density of nucleation sites indicates that the silicon nanocrystallites are very small in size but their density is high. The energy gap is increased by decreasing the size of silicon nanocrystallites.

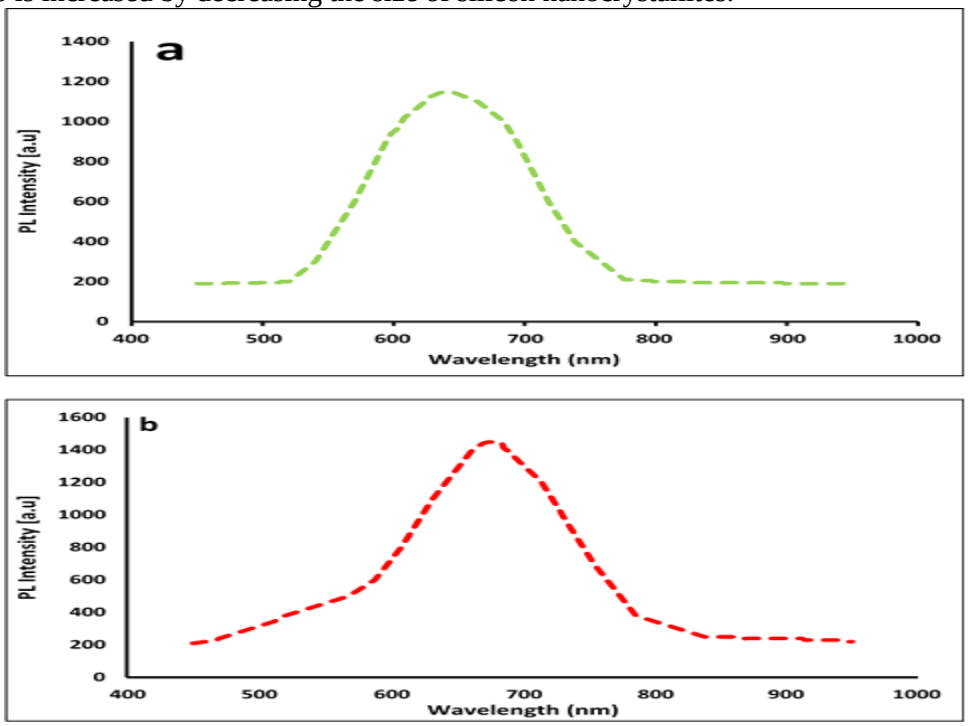

Figure 3-PL spectrum of the based PSi layer of Si wafer resistivity at a) 10 Ω.cm (pores-like structures) and b) 100 Ω.cm (mud-like structures).

Table 1-The obtained results from the analysis of the PL spectra

Morphological structure	***Peak wavelength(nm)***	***PL peak intensity (a.u)***	***PSi energy gap (ev)***	***Si nano size (nm)***
Mud-like structure	638	1450	1.943	29.71
Pores-like structure	680	1150	1.82	34.16

3-3 Characterization of plasmonic Au-NPs hot spot SERS sensors

The characterization of plasmonic Au-NPs/PSi hot spot SERS sensors is very important to recognize the performance of these sensors. The performance of theses sensors was extensively studied through the analysis of the morphological and structural properties as well as Raman spectroscopy of the sensors at the fixed amoxicillin concentration of 10^{-3}M. The SERS sensors were dipped into the prepared solution of amoxicillin for ten hours in dark at room temperature.

3-4 Morphological aspects of plasmonic Au-NPs hot spot SERS sensors

Plasmonic Au-NPs hot spot layer was examined as an efficient SERS sensor for the detection of amoxicillin based morphological aspects of both types of PSi (pores- like and mud- like structures). The influence of the size of the Au-NPs and the density of the hot spot regions on the performance of the SERS sensor was investigated. The sensor behavior varies with the structures of the base porous layer. Figure-4 shows the SEM of plasmonic Au-NPs/PSi hot spot SERS sensors based on the pores-like structures. The morphological aspect of the deposited Au-NPs over the Si of pores-like structures shows that the form of the nanoparticles appears as spherical, semi-isolated, nanoparticles with different sizes over the nano columns layer. These formed nanoparticles complete only a single layer over the pore structures which subsequently form a homogeneous growth, where the layer contains low density of Si– H_x bond.

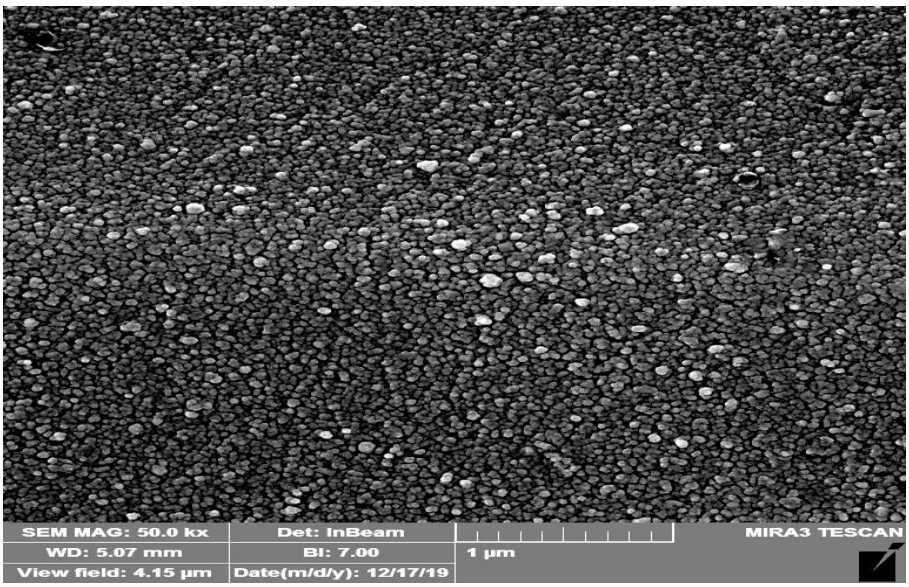

Figure 4-Morphological aspects of plasmonic Au-NPs/PSi hot spot SERS sensors based on the pores –like structures.

For the pores-like structures, the dimension sizes of plasmonic Au-NPs and the density of hot spot regions among the nanoparticles fluctuated with the morphological aspects. Figure-(5 a, b) illustrates the size of plasmonic Au-NPs and the hot spot regions among the Au-NPs, respectively. The formation and density of the hot spot regions depends on the PSi morphology, since the structure has high nucleation site and high density of the hot spot regions. The histogram of plasmonic Au-NP size ranged from 10 to 70 nm, whereas the peak of the size was about 20 nm with a percentage of about 35%. The histogram of the hot spot gaps (vacancies) among the plasmonic Au-NPs ranged from 46 to 58 nm with the highest peak being located at 58 nm with a percentage of about 23%.

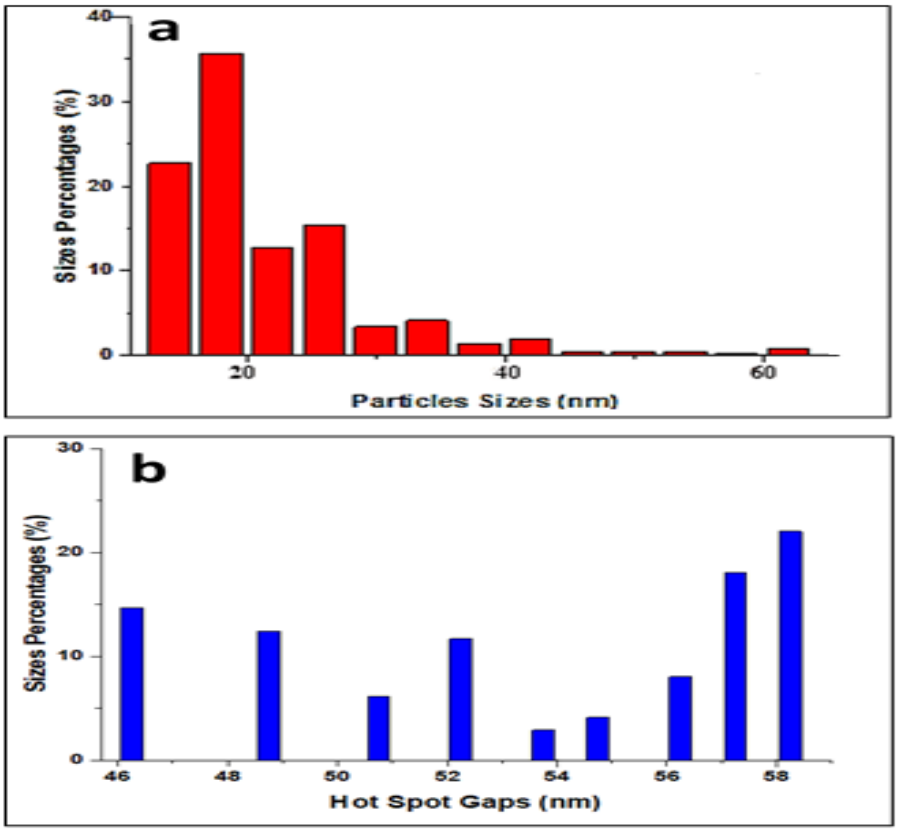

Figure 5a, b: The sizes of plasmonics Au-NPs/PSi hot spot SERS sensors and hot spot gaps among them for pores-like structures.

For mud-like structures, Figure-6 shows the FE-SEM of plasmonic Au-NPs/PSi hot spot SERS sensors. The morphological features of the Au-NPs deposited above the Si of mud-like structures displayed aggregated NPs with a nearly cauliflower-like form and different sizes. These formed nanoparticles completed more than a single layer over the mud structures which subsequently form a non-homogeneous growth, where the layer contains a high density of Si– H_x bond.

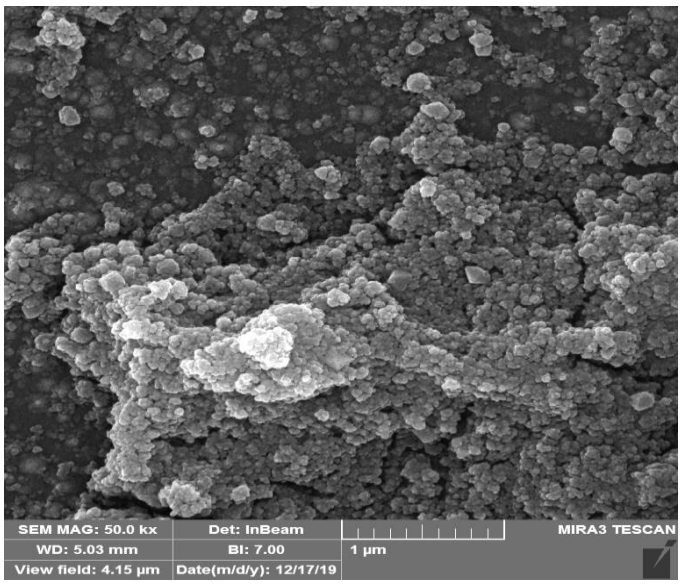

Figure 6- Morphological aspects of plasmonic Au-NPs / PSi hot spot SERS sensor for mud- like structures.

The size histogram of plasmonic Au-NPs and the density of the hot spot gaps among the nanoparticles deposited above the mud layer are illustrated in Figure-7 a, b, respectively. The size of the Au-NPs ranged from 20 to 120 nm, whereas the highest proportion of these NPS (39%) was of the size of 10 nm. Also, the size of the hot spot gaps (vacancies) among the Au-NPs ranged from 36 to 45 nm, while the highest peak was located at 45 nm with a percentage of about 23%. These sizes of the formed hot spot gaps for mud-like structures were lower than those of the pores-like structures. The density of the synthesized nano-gaps (Raman active sites) for the porous layer of mud-like structures, which was originated by 30% laser duty cycles, was higher than that of the others types of porous layers. Thus, we expect that the resulted SERS spectrum is increased with the percentage of this active site.

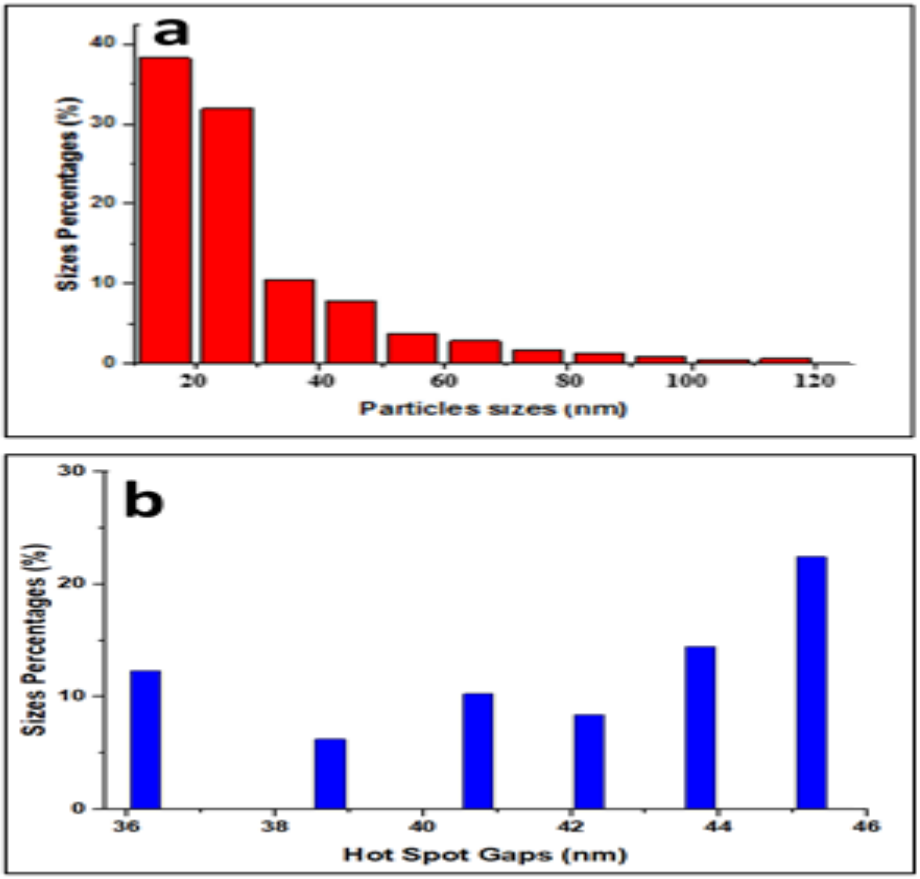

Figure 7a, b-The size of Plasmonics Au-NPs/PSi hot spot SERS and hot spot gaps among them for mud- like structures.

3-5 Detection of the performance of plasmonic AuNPs hot spot SERS sensors based on the bare PSi

The sensing performance of the bare pores-like and mud- like structures was firstly inspected at the higher concentration of amoxicillin of about 10^{-1} M in order to recognize the effects of PSi morphologies on the detection process of amoxicillin solution. Figure-8(a, b) illustrates the measured Raman Spectra of bare PSi at a fixed concentration of amoxicillin of about 10^{-1} M for both types of morphologies. The measured Raman spectra of mud-like structures for the amoxicillin solution were higher than those of pores-like structures. The analysis of Raman spectrum of amoxicillin showed the presence of main peak intensity of about 1592 cm^{-1} and 968cm^{-1}. These characteristic peaks can be used for a qualitative analysis of amoxicillin due to the positive correlation with its concentration. In addition to these characteristics, there were other Raman peaks of wave numbers of 850 and 1420 cm^{-1}. These measured peaks are in excellent agreement with those obtained by Ji *et al*. [21]. The intensity of the main peak is very small and, thus, the incorporation of bare PSi with Au-NPs was employed to develop SERS enhancement ability.

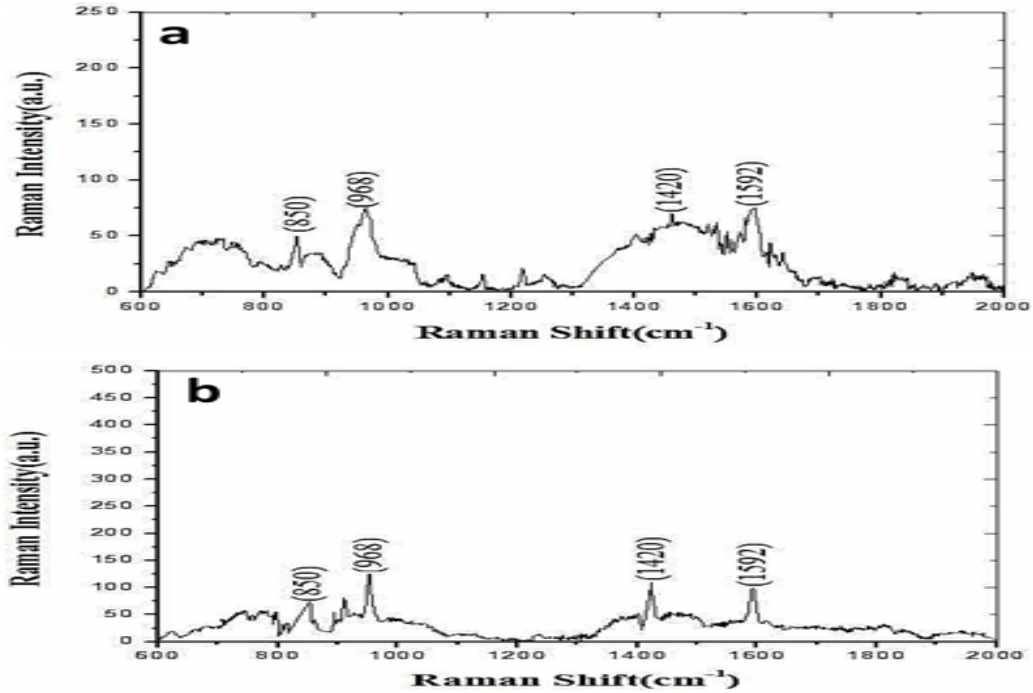

Figure 8-Raman spectra of bare PSi for amoxicillin at fixed concentration of about 10^{-1} M, a) pores-like structures, b) mud-like structures.

The sensing performance of the plasmonic Au-NPs hot spot SERS sensors was inspected at a lower concentration of about 10^{-3} M of amoxicillin for depositing Au-NPs on both PSi morphologies (pores- like and mud- like structure), as shown in Figure-9(a,b).

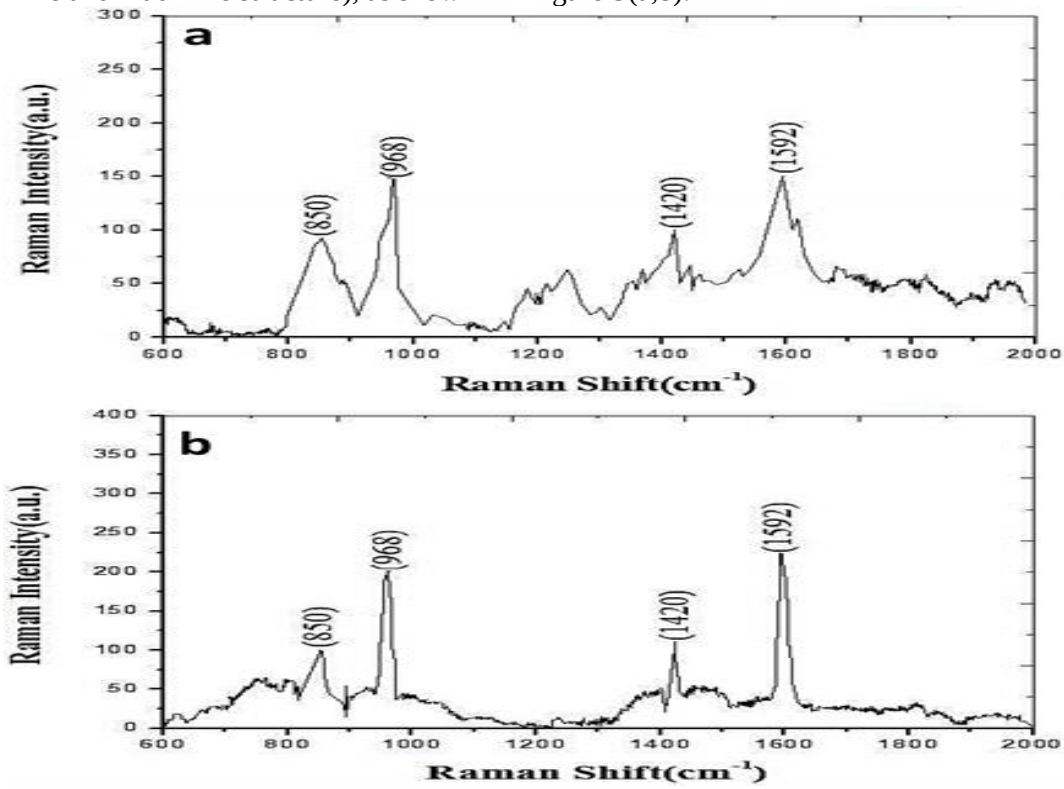

Figure 9-SERS spectra of plasmonic Au-NPs/PSi hot spot SERS sensors for amoxicillin at a fixed concentration of about 10^{-3} M, based on a) pores-like structures, b) mud-like structures.

From this figure, we observe that the increase of Raman intensity of the main peak of hot spot SERS sensor based on the pores-like structure was much lower than that of the hot spot SERS sensor based on the mud-like structure. This is strongly related with the density and the size of the formed hot

spot regions. Based on the analysis of the obtained micro images of the scanning electron microscopy, the hot spot gaps had a higher population at higher gap sizes. This would inhibit or reduce the coupling efficiency between the local antenna and the target molecules inside the hot spot regions. The decrease of this efficiency would lead to decrease the obtained Raman signal due to the decrease in the absorbed photon by the target molecules. The density and size of the hot spot gaps among the plasmonic Au-NPs play a considerable role in the performance of the SERS sensors [22,23]. Assume that two nanoparticles of size (D) are separated by gap (hot spot gap) of size (d). If these nanoparticles are presented in an uniform electrostatic field (E_0) of Raman signal , the contingent local electric field (E_L) will vary with the nanoparticle size and the hot spot gap size, as given by the following equation [23] .

$$E_L = E_0\big((D + d)/d\big) \quad (2)$$

When a molecule of antibiotics is located in these hot spot gaps, an improvement in the intensity of the Raman signal will be attained by Surface Plasmonics (SP). This dependence of the performance of SERS sensor on the hot spot gaps is in excellent agreement with the results observed by Wali *et al*. [22].

In order for the comparison to be complete, it is better to calculate the enhancement factor (EF) using the following equation [22]:

$$EF = (I_{SERS} \times C_R)/(I_R \times C_{SERS}) \quad (3)$$

where I_{SERS} is the SERS intensity of plasmonic hot spot SERS sensors and I_R is the Raman intensity of the bare PSi (mud-like s and pores-like structures) at the amoxicillin concentrations of C_{SERS} and C_R, respectively. The EF values of hot spot SERS sensor based on both types of PSi morphologies were about 250 and 175 for 10^{-3} M of amoxicillin at the main peak of 1592 cm^{-1}, respectively. This confirms that the plasmonic Au-NPs hot spot SERS based on the mud-like structures has higher sensitivity than that based on the pores-like structures.

Conclusions

Efficient, low cost, and easy to fabricate plasmonic Au-NPs hot spot SERS sensors were developed based on both PSi morphologies (pores-like and mud-like structures) for the detection of amoxicillin. The best detection conditions which involve higher sensitivity and excellent linearity were achieved for the sensor based on PSi morphology with mud- like structures.

Acknowledgments

The authors would like to thank the University of Technology, Baghdad-Iraq, for their support in the present work.

References

1. Li R, Zhang H, Chen Q-W, Yan N. and Wang H. **2011**. Improved surface-enhanced Raman scattering on micro-scale Au hollow spheres: Synthesis and application in detecting tetracycline. *Analyst,* **136**(12): 2527-2532. https://doi.org/10.1039/C1AN15195A.
2. Dong R, Weng S, Yang L, Liu J. **2015**. Detection and direct readout of drugs in human urine using dynamic surface-enhanced Raman spectroscopy and support vector machines. *Analytical chemistry*, **87**(5): 2937-2944. https://doi.org/10.1021/acs.analchem.5b00137.
3. Chen Y, Li X, Yang M, Yang L, Han X, Jiang X, Zhao B. **2017**. High sensitive detection of penicillin G residues in milk by surface-enhanced Raman scattering. *Talanta*, **167**: 236-241. https://doi.org/10.1016/j.talanta.2017.02.022.
4. Xie Y, Zhu X, Sun Y, Wang H, Qian H, Yao W. **2012**. Rapid detection method for nitrofuran antibiotic residues by surface-enhanced Raman Spectroscopy. *European Food Research and Technology*, **235**(3): 555-561 https://doi.org/10.1007/s00217-012-1752-5.
5. Zhao J, Liu P, Yuan H, Peng Y, Hong Q, Liu M. **2016**. Rapid detection of tetracycline residues in duck meat using surface enhanced raman spectroscopy. *Journal of Spectroscopy*, 2016. http://dx.doi.org/10.1155/2016/1845237.
6. Dhakal S, Chao K, Huang Q, Kim M, Schmidt W, Qin J, Broadhurst CL. **2018**. A simple surface-enhanced Raman spectroscopic method for on-site screening of tetracycline residue in whole milk. *Sensors,* **18**(2): 424. https://doi.org/10.3390/s18020424.7.

7. Wali LA, Hasan KK, Alwan AM. **2020**. An Investigation of Efficient Detection of Ultra-Low Concentration of Penicillins in Milk Using AuNPs/PSi Hybrid Structure. *Plasmonics*:1-9. https://doi.org/10.1007/s11468-019-01096-4.

8. Ranjan M. and Facsko S. **2012**. Anisotropic surface enhanced Raman scattering in nanoparticle and nanowire arrays. *Nanotechnology*, **23**(48): 485307. https://doi.org/10.1088/0957-4484/23/ 48/ 485307.

9. Le Ru E. and Etchegoin P. **2008**. P*rinciples of Surface-Enhanced Raman Spectroscopy: and related plasmonic effects*. Elsevier,

10. Baia M, Astilean S. and Iliescu T. **2008**. *Raman and SERS investigations of pharmaceuticals*. Springer Science & Business Media,

11. McQuillan AJ. **2009**. Recollection. The discovery of surface-enhanced Raman scattering: Notes Rec. R. Soc. 63, 105–109 (20 March 2009; Published online 6 January 2009)(doi: 10.1098/rsnr. 2008.0032). *Notes and Records of the Royal Society*, **63**(2): 209-209.

12. Qi M, Huang X, Zhou Y, Zhang L, Jin Y, Peng Y, Jiang H, Du S. **2016**. Label-free surface-enhanced Raman scattering strategy for rapid detection of penicilloic acid in milk products. *Food chemistry*, **197**: 723-729. https://doi.org/10.1016/j.foodchem.2015.11.014

13. Alwan AM, Hashim DA, Jawad MF. **2018**. Optimizing of porous silicon alloying process with bimetallic nanoparticles. *Gold Bulletin*, **51**(4): 175-184. https://doi.org/10.1007/s13404-018-0242-3.

14. Wali LA, Alwan AM, Dheyab AB, Hashim DA. **2019**. Excellent fabrication of Pd-Ag NPs/PSi photocatalyst based on bimetallic nanoparticles for improving methylene blue photocatalytic degradation. *Optik*, **179**: 708-717. https://doi.org/10.1016/j.ijleo.2018.11.011.

15. Alwan AM, Wali LA, Yousif AA. **2018**. Optimization of AgNPs/mesoPS active substrates for ultra–low molecule detection process. *Silicon*, **10**(5): 2241-2251. https://doi.org/10.1007/s12633-018-9758-7.

16. Alwan AM, Yousif AA. and Wali LA. **2017**. The growth of the silver nanoparticles on the mesoporous silicon and macroporous silicon: a comparative study. *Indian Journal of Pure & Applied Physics* (IJPAP), **55**(11): 813-820.http://op.niscair.res. in/index.php/IJPAP /article/ view/ 15477

17. Alwan AM, Yousif AA, Wali LA. **2018**. A study on the morphology of the silver nanoparticles deposited on the n-type porous silicon prepared under different illumination types. *Plasmonics*, **13** (4): 1191-1199. https://doi.org/10.1007/s11468-017-0620-3

18. Alwan AM, Naseef IA. **2017**. Optimization of photoluminescence properties of Porous silicon by adding gold nanoparticles. *Iraqi Journal of Science*, **58**(1A): 53-62.

19. Alwan AM, Abbas RA, Dheyab AB. **2018**. Study the characteristic of planer and sandwich PSi gas sensor (Comparative Study). *Silicon*, **10**(6):2527-2534. https://www.iasj.net/iasj? func= article &aId =123222

20. Ismail RA, Khashan KS, Alwan AM. **2017**. Study of the effect of incorporation of CdS nanoparticles on the porous silicon photodetector. Silicon, **9**(3): 321-326. https://doi.org/10.1007 /s12633-016-9446-4.

21. Ji W, Wang L, Qian H. and Yao W. **2014**. Quantitative analysis of amoxicillin residues in foods by surface-enhanced Raman spectroscopy. *Spectroscopy Letters*, **47**(6):451-457. https://doi.org/ 10. 1080/00387010.2013.807843.

22. Wali LA, Hasan KK, Alwan AM. **2019**. Rapid and highly efficient detection of ultra-low concentration of penicillin G by gold nanoparticles/porous silicon SERS active substrate. *Spectrochimica Acta Part A: Molecular and Biomolecular Spectroscopy*, **206**: 31-36. https:// doi.org/10.1016/j.saa.2018.07.103019.

23. Jabbar AA, Alwan AM. and Haider AJ. **2018**. Modifying and fine controlling of silver nanoparticle nucleation sites and SERS performance by double silicon etching process. *Plasmonics*, **13**(4): 1171-1182. https://doi.org/10.1007/s11468-017-0618-x.